Herpesvirus infection reduces Pol II occupancy of host promoters but spares viral promoters

Ella N Hartenian[1], Britt A Glaunsinger[1,2,3,*]

[1]Department of Molecular and Cell Biology, University of California Berkeley, CA, USA

[2]Department of Plant and Microbial Biology, University of California Berkeley, CA, USA

[3]Howard Hughes Medical Institute, University of California Berkeley, CA, USA

*Corresponding author

Email: glaunsinger@berkeley.edu

Abstract

In mammalian cells, widespread acceleration of cytoplasmic mRNA degradation is linked to impaired RNA polymerase II (Pol II) transcription. This mRNA decay-induced transcriptional repression occurs during infection with gammaherpesviruses including Kaposi's sarcoma-associated herpesvirus (KSHV) and murine gammaherpesvirus 68 (MHV68), which encode an mRNA endonuclease that initiates widespread RNA decay. Here, we show that MHV68-induced mRNA decay leads to a genome-wide reduction of Pol II occupancy at mammalian promoters. Viral genes, despite the fact that they require Pol II for transcription, escape this transcriptional repression. Protection is not governed by viral promoter sequences; instead, location on the viral genome is both necessary and sufficient to escape the transcriptional repression effects of mRNA decay. We hypothesize that the ability to escape from transcriptional repression is linked to the localization of viral DNA in replication compartments, providing a means for these viruses to counteract decay-induced viral transcript loss.

Introduction

Regulating messenger RNA (mRNA) abundance is of central importance during both cellular homeostasis and disease. While it is intuitive that transcriptional changes in the nucleus impact RNA levels in the cytoplasm, evidence in both yeast and mammalian cells now indicates that the converse is also true: altered cytoplasmic mRNA decay rates can broadly impact transcription by RNA polymerase II (Pol II). In yeast, stabilizing the cytoplasmic mRNA pool by removing mRNA decay factors such as Xrn1 causes a compensatory decrease in Pol II transcription (1-5). Furthermore, reducing or slowing Pol II transcription leads to an increase in

50 overall mRNA stability (1), supporting a “buffering” model in which yeast can compensate for
51 widespread perturbations to mRNA abundance by alternatively changing rates of transcription.
52 Broad changes in mRNA abundance are often triggered in mammalian cells during viral
53 infection. Numerous viruses, including alphaherpesviruses, gammaherpesviruses, SARS
54 coronavirus and influenza A virus drive accelerated mRNA decay during infection by expressing
55 mRNA specific endoribonucleases and/or activating host nucleases. This decay contributes to
56 viral immune evasion, increases the availability of host translation machinery, and facilitates
57 temporal viral gene regulation (6-10). Viral endonucleases target host and viral mRNAs for
58 cleavage, whereupon cellular exonucleases degrade the resulting mRNA fragments (11-15). This
59 strategy accelerates basal RNA decay by circumventing the typically rate limiting steps of
60 deadenylation and decapping (16-20).
61 Although yeast and mammals share key proteins involved in cytoplasmic mRNA decay
62 and transcription, studies with RNA-decay inducing viruses in mammals have revealed that
63 unlike the yeast pathway, accelerated mRNA decay leads to an extensive shutoff of cellular gene
64 expression (21,22). Infection with the gammaherpesviruses KSHV or MHV68 causes reduced
65 Pol II recruitment at host promoters in a manner dependent on mRNA cleavage by the viral
66 endonucleases SOX or muSOX. Thus, accelerated mRNA decay is not broadly counteracted by
67 increased transcription-based repopulation, but instead leads to a more extensive shutdown of
68 cellular gene expression. However, similar to yeast, the mammalian connection between decay
69 and transcription requires the activity of cellular exonucleases such as Xrn1, which degrade the
70 viral endonuclease cleavage products (16,21). Accelerated Xrn1-mediated degradation causes
71 trafficking of released RNA binding proteins (RBP) from the cytoplasm to the nucleus, which
72 may provide a means for the cell to detect and respond to increased RNA turnover (22).

73 During MHV68 infection, in addition to host mRNA, cytoplasmic viral mRNA is
74 susceptible to cleavage by muSOX (23). However, measurements of nascent transcript
75 production from a subset of viral promoters suggested that viral genes are robustly transcribed
76 during the stage of infection when host transcription is reduced (24). An outstanding question is
77 how these viral promoters escape mRNA decay-induced transcriptional repression despite being
78 transcribed by RNA Pol II. Here, we measured Pol II occupancy across the mouse and MHV68
79 genomes in infected cells to more comprehensively define how accelerated mRNA decay
80 impacts polymerase occupancy. Our data demonstrate a genome-wide reduction in Pol II
81 recruitment at host promoters under conditions of increased mRNA decay. In contrast, Pol II
82 occupancy of the viral genome appears broadly resistant to the effects of mRNA degradation.
83 This protection is not conferred by viral promoter sequences; instead, location on the replicating
84 viral genome is both necessary and sufficient to escape the transcriptional effects of mRNA
85 decay. We propose a model in which DNA amplified in viral replication compartments, unlike
86 the cellular chromatin, is immune to transcriptional repression during accelerated cytoplasmic
87 mRNA decay. Thus, while both viral and cellular mRNA pools are susceptible to cytoplasmic
88 degradation, transcriptional repopulation selectively counteracts this loss for viral genes.
89

90 ## Results

91 **Accelerated RNA decay broadly reduces Pol II occupancy**

92 We previously reported that Pol II occupancy at several individual mammalian promoters
93 was significantly reduced during accelerated cytoplasmic mRNA decay (22,24). To more
94 comprehensively assess the extent of mRNA decay-induced transcriptional repression, we
95 evaluated global Pol II occupancy by chromatin immunoprecipitation and deep sequencing

96 (ChIP-seq) in mock versus MHV68 infected MC57G mouse fibroblasts at 24 hours post
97 infection (hpi). As a control, we also infected cells with a version of MHV68 containing the
98 point mutation R443I in the viral muSOX endonuclease gene, which reduces its mRNA cleavage
99 activity. R443I retains a similar lytic cycle and infectious capability to wildtype (WT) MHV68 *in*
100 *vivo* and in vitro its infectious capability is similar to MHV68 in mouse fibroblasts (6,23).
101 MHV68-infected cells displayed promoter-proximal loss of Pol II at 86% of loci compared to
102 mock-infected cells, averaged across two biological replicates and subtracting input signal (Fig
103 1A and S1 Fig A). Loss of Pol II occupancy was primarily due to muSOX-induced mRNA
104 decay, as this signal loss either did not occur or was reduced at 67% of these loci during
105 infection with R443I MHV68 (Fig 1A and S1 Fig A). Sixty-three genes, or 1.3% of loci, showed
106 higher Pol II occupancy in WT infection as compared to mock infection, although these did not
107 share any common GO terms (S1 Table). A representative genome browser view shows reduced
108 Pol II signal throughout *Srsf2* in the MHV68 condition of two replicate ChIP experiments. We
109 independently validated the ChIP-seq results by ChIP-qPCR at the *Rplp0* and *Fus* promoters,
110 both of which showed a significant reduction of Pol II occupancy in cells infected with WT but
111 not R443I MHV68 (Fig 1C), as did a validation using a second antibody that recognizes the N-
112 terminus of the major subunit of Pol II, Rpb1 (Fig1D). The genome-wide reduction in poised Pol
113 II in WT but not R443I infected cells was also evident when the sequencing reads from positions
114 -2000 to +4000 around the transcription start sites (TSS) were plotted as a histogram (Fig 1G and
115 S1 Fig B). The variability between replicates in R443I recovery (Fig 1B) is likely due to
116 differences in the extent of host shutoff reduction between replicates due to R443I reducing
117 muSOX activity while not being a catalytic mutant.

118 To assess the stage of transcription impacted by RNA decay, we compared the amount of
119 Pol II in promoter regions (-50 to +200) and the amount of Pol II in gene bodies (+200 to +5000)
120 between mock and infected samples. Consistent with the above analyses, MHV68 infected cells
121 contained markedly less promoter proximal Pol II than uninfected cells, and this signal was
122 partially recovered in the R443I infection (Fig 1E). Genes with impaired Pol II promoter binding
123 during MHV68 infection also had less Pol II within the gene body compared to mock infected
124 cells, which again was not observed during R443I infection (Fig 1F). Notably, the difference in
125 regression line slopes between MHV68 and mock infected cells was clearly more marked when
126 comparing Pol II promoter occupancy, suggesting that the primary transcriptional defect is at the
127 stage of initiation. This is consistent with data from previous studies that found no defect in
128 serine 2 phosphorylation of elongating Pol II and no consistent change to Pol II elongation
129 during MHV68 infection (22,24).
130 Finally, to assess if RNA decay affected transcription termination, we plotted sequencing
131 reads between 1kb upstream and 1kb downstream of the transcription termination site (TTS) as a
132 histogram (Fig 1H and S1 Fig D). TTS-proximal Pol II shows no defect in termination in either
133 infection condition, suggesting Pol II removal from host transcripts is not impacted by MHV68
134 infection or by RNA decay.
135
136 **Pol II recruitment to viral genes is not affected by RNA decay**
137 Herpesviral genes are transcribed in the nucleus by mammalian Pol II, and thus could be
138 similarly subjected to the mRNA decay-induced transcriptional repression observed across the
139 host genome. We therefore analyzed Pol II occupancy of the viral genome in WT MHV68 and
140 R443I infected cells to determine how viral genes respond to RNA decay. The average Pol II

141 signature across 82 viral ORFs between -500 and +500 around the TSS was comparable in cells
142 infected with WT or R443I MHV68, with a slightly higher signal in the R443I infection (Fig
143 2A). Indeed, there was a robust and widespread Pol II signal in both infection conditions across
144 the viral genome (Fig 2B). Thus, herpesviral genes appear to escape mRNA decay-induced
145 transcriptional repression.

146 In contrast to host genes, we did not observe peaks of promoter-proximal Pol II on the
147 viral genome in our ChIP-seq data (Fig 2A and B). Pol II ChIP qPCR across various regions of
148 ORF54 and ORF37 also showed a similar Pol II signal throughout each gene body and at their
149 promoter. We did note a decrease in signal near the TTS of ORF54, however this was true for
150 both WT and R443I infections (Fig 2C). We hypothesize that pervasive transcription of the viral
151 genome at 24 hpi, compounded by the presence of TSSs on both Watson and Crick strands,
152 likely contributes to this phenotype.

153

154 **PABPC is not excluded from viral replication compartments**

155 We next considered how the viral genome maintains high levels of Pol II occupancy
156 during accelerated mRNA decay. During replication, viral DNA is transcribed within viral
157 replication compartments (RCs) in the nucleus, which exclude host DNA and thus stain poorly
158 with DAPI (25-27). Although they are not membrane bound, these compartments selectively
159 enrich for factors required for viral replication (such as the viral processivity factor ORF59) and
160 gene expression (such as Pol II) (28-30). Virus-induced mRNA decay causes increased
161 trafficking of cytoplasmic poly(A) binding protein (PABPC) from the cytoplasm to the nucleus,
162 which we have recently linked to transcriptional repression (22,31). To determine whether
163 replication compartments selectively exclude nuclear PABPC as a means of avoiding

164 transcriptional repression, we monitored its localization in cells lytically infected with MHV68
165 or KSHV. As expected, the majority of infected cells displayed increased nuclear PABPC
166 compared to unreactivated or uninfected cells as measured by immunofluorescence (IF). We
167 further saw that PABPC was not excluded from replication compartments (Fig 3A, B and S2 Fig
168 A). To determine PABPC localization relative to RCs, we first identified cells with RCs by
169 looking for regions of Pol II or ORF59 staining that excluded DAPI. We then quantified nuclear
170 PABPC pixel intensity, and counted cells as having an overlapping RC/PABPC signal when the
171 PABPC pixel intensity was at least 2x that of cells without nuclear PABPC from the same image.
172 Indeed, 85 percent of MHV68 infected cells showed overlapping PABPC/Pol II signal and 90
173 percent of reactivated iSLKs showed an overlapping PABPC/ORF59 signal (Fig 3C). Thus,
174 PABPC exclusion from RCs is unlikely to underlie viral promoter escape.
175
176 **Viral promoters fail to escape transcriptional repression outside of the viral genome**
177 We then tested whether viral promoter sequence elements were sufficient to enable
178 escape by querying whether they conferred resistance to transcriptional repression upon
179 relocation from the viral genome into the host DNA. We inserted the MHV68 late promoter M7
180 or the KSHV LANA promoter upstream of a puromycin resistance cassette into 293T cell
181 chromatin using either lentiviral transduction or random plasmid DNA integration, respectively.
182 We induced mRNA decay and host transcriptional repression in these cells by expression of
183 MHV68 muSOX or the herpes simplex virus type 1 (HSV-1) endonuclease vhs. Similar to the
184 host promoters *Gapdh* and *Rplp0*, Pol II recruitment to both integrated viral promoters was
185 repressed upon infection with MHV68 but not with R443I (Fig 4A and 5B).

186 To confirm that viral promoters integrated into the host genome were also repressed in
187 the context of infection, we infected MC57G cells containing an integrated MHV68 M4
188 promoter-driven puromycin cassette with MHV68. Indeed, the M4 promoter was repressed to a
189 similar degree as host *Fus* and *Rplp0* promoters during infection with WT MHV68 but not the
190 mRNA decay-deficient MHV68 R443I (Fig 4C). In summary, these data argue against the
191 presence of protective elements within viral promoters, and instead suggest that the chromatin
192 context or location on the viral genome underlies escape from mRNA decay-induced
193 transcriptional repression.
194
195 **Non-MHV68 promoters escape repression on the viral genome**
196 A prediction from the above results is that non-MHV68 promoters would gain protection
197 from transcriptional repression when present on the replicating viral genome. To test this, we
198 measured the Pol II occupancy and transcriptional potential of the cytomegalovirus (CMV)
199 promoter, which drives green fluorescent protein (GFP) expression on the MHV68 genome.
200 Unlike alpha- and gammaherpesviruses, the betaherpesvirus CMV does not accelerate mRNA
201 decay. Furthermore, in either a plasmid context or when integrated into 293T cells, the CMV
202 promoter is strongly repressed during muSOX-induced mRNA decay. This is seen by 4SU
203 incorporation measuring nascent RNA production - similar to the control *ActB* gene - and by Pol
204 II recruitment, similar to the control *Fus* and *Rplp0* promoters (Fig 5A and B). However, in the
205 context of the replicating MHV68 genome, the CMV-GFP promoter had a Pol II ChIP-seq signal
206 during both MHV68 WT and R443I infection that was not markedly different from several other
207 viral genes (ORFs 4, 25, 48, 52, 72, M11) (Fig 5C).

208 Finally, we evaluated whether the lytic stage of infection was necessary to confer escape
209 from transcriptional repression, or whether some other feature of the non-replicating viral
210 genome was important. To this end, we examined Pol II occupancy at promoters of several genes
211 expressed from the KSHV genome during latent infection in 293T cells, when the viral DNA is
212 maintained as an episome but not amplified in replication compartments. Latent infection does
213 not promote mRNA turnover, and thus we transfected muSOX into these cells to stimulate
214 mRNA turnover in the absence of lytic replication. Similar to the host genes *Gapdh* and *Rplp0*,
215 we observed an RNA decay-induced repression of Pol II occupancy at the latent viral promoter
216 LANA while the viral K1 promoter was repressed in 4 out of 5 experiments (Fig 5D). We also
217 observed repression of the human *Ef1α* promoter, which is present on the KSHV viral episome
218 as a driver of the GFP reporter gene (Fig 5D). In sum, these observations indicate that the viral
219 genome per se does not confer protection from transcriptional repression; instead, features linked
220 to lytic genome amplification in replication compartments facilitate robust Pol II recruitment
221 under conditions of accelerated mRNA turnover.
222

223 **Discussion**

224 Here, we demonstrate that virus-induced mRNA decay broadly decreases Pol II
225 recruitment to mammalian promoters, extending prior observations made with individual cellular
226 genes to the genomic scale. In contrast, promoters on the replicating viral genome recruit Pol II
227 with similar efficiency during normal or accelerated mRNA decay, indicating that they escape
228 transcriptional inhibition. This protection is lost upon relocation of the viral promoters into the
229 host genome or when the viral genome is in a latent state, emphasizing the importance of DNA

230 context and replication state, rather than promoter sequence, in determining the transcriptional
231 response to accelerated mRNA decay.

232 Across the host genome, Pol II appears to be most strongly affected at the stage of
233 recruitment. The reduction in promoter-proximal Pol II is propagated into the gene body,
234 although the differences there were less pronounced, suggesting that once transcription of a gene
235 initiates there are not subsequent blocks to elongation. This agrees with prior studies of
236 individual host loci in MHV68 infected or muSOX expressing cells (22,24). The population of
237 Pol II that is promoter-proximal and measured during a ChIP experiment has been shown to
238 comprise a combination of actively engaged Pol II as well as Pol II transiently binding to the
239 DNA. Thus, a large reduction in promoter-proximal Pol II may not be expected to be borne out
240 in the gene body (32). Additionally, the antibody we use in this study binds with higher affinity
241 to hypophosphorylated Pol II(33), likely affecting our ability to pull down elongating and
242 phosphorylated forms of Pol II. We also did not observe a defect in transcription termination, or
243 evidence of polymerases on the DNA after TTSs, suggesting that the gammaherpesvirus MHV68
244 does not induce the termination defect and run-on transcription of host genes recently described
245 in HSV-1 (34).

246 Two pieces of evidence indicate that reduction of Pol II at host genes is unlikely due to
247 sequestration of or competition for the transcription machinery by the viral DNA. First, infection
248 with the mRNA decay mutant virus R443I, which replicates its viral genome to WT levels (6),
249 does not induce the widespread reduction in Pol II recruitment to host promoters. Second,
250 transfection of muSOX alone (or other broad acting viral endonucleases) in the absence of viral
251 infection is sufficient to induce transcriptional repression at host promoters. Therefore, we
252 instead favor the hypothesis that one or more cellular proteins released from degrading mRNA

253 fragments triggers a signaling event that restricts transcription machinery occupancy of
254 mammalian chromatin (22).
255 Reduced Pol II occupancy of the host genome during MHV68 infection parallels
256 infection data from the alphaherpesvirus HSV-1. HSV-1 infection results in a genome-wide
257 reduction in Pol II occupancy of host chromatin and reduced nascent RNA production of the
258 majority of host transcripts (34-36). Furthermore, early data showed that while the endogenous
259 mouse β-globin locus was transcriptionally repressed during HSV-1 infection, its expression was
260 rescued upon integration of the β-globin gene into the HSV-1 genome (37,38). Experiments with
261 gene-specific null viruses have implicated immediate early (IE) proteins in the HSV-1
262 transcriptional repression phenotype, including ICP27, which can accelerate mRNA turnover
263 (36,39). Additionally, we have previously published, and confirm in this report, that transfection
264 of HSV-1 vhs, another broad acting endoribonuclease, is sufficient to induce reduced Pol II
265 occupancy of several host promoters (21). Thus, in addition to targeting host and viral mRNAs
266 for cytoplasmic decay, both alpha and gammaherpesviruses restrict Pol II occupancy of the host
267 genome, although additional work is needed to establish whether the underlying mechanism is
268 similar.
269 During the lytic stage of herpesvirus infection, viral DNA is localized to replication
270 compartments. These non-membrane bound structures are sites of viral genome replication,
271 transcription, and packaging (40). They are enriched for many host and viral proteins involved in
272 these processes, including chromatin modifying factors and Pol II (28-30). Replication
273 compartments grow and coalesce over infection, excluding host chromatin, which becomes
274 pushed to the nuclear periphery (25-27). We recently showed that muSOX and Xrn1-coordinated
275 mRNA decay causes differential trafficking of many cellular RNA binding proteins between the

276 cytoplasm and nucleus. Knockdown and overexpression studies suggested that at least one of
277 these proteins, PABPC, is associated with transcriptional repression (22). Here, we detected
278 PABPC in viral replication compartments of infected cell nuclei, indicating that selective
279 exclusion of PABPC from these compartments is not the mechanism by which the viral genome
280 escapes repression. Instead, we hypothesize that either the state of viral DNA or other protective
281 features of the replication compartment confers escape from transcriptional repression.

282 Protection from mRNA decay-induced transcriptional repression was not conferred to
283 non-MHV68 or viral promoters present on the latent viral episome, indicating that lytic phase
284 viral DNA replication or replication compartment formation is key to this phenotype. The latent
285 genomes of gammaherpesviruses including KSHV and Epstein Bar Virus (EBV) are heavily
286 methylated and histone-rich, with the exception of promoters of genes expressed during latency,
287 the latent origin of replication, and CTCF binding sites (41-43). Notably, during latency key lytic
288 promoters like RTA contain both the activating H3K4me3 and the repressive H3K27me3 histone
289 marks, representing a 'poised' state (44). Rapid changes shortly after lytic cycle induction result
290 in hypomethylation and removal of repressive marks at early gene promoters (41,44). At later
291 stages of infection, KSHV, EBV and HSV-1 genomes have been shown to be largely
292 nucleosome free, consistent with histones not being packaged in virions (27,29,45). For
293 gammaherpesviruses, this is the stage at which mRNA degradation is most pronounced. We
294 therefore hypothesize that the 'open' state of viral DNA during lytic replication plays an
295 important role in facilitating Pol II recruitment under conditions of accelerated cytoplasmic
296 mRNA decay. Future work is geared towards exploring whether widespread mRNA decay alters
297 cellular chromatin states and DNA accessibility and, if so, how this influences transcription
298 factor recruitment.

299 In conclusion, decay-coupled transcriptional repression is a novel facet of viral
300 manipulation of the cellular gene expression landscape. We hypothesize that the ability to escape
301 from transcriptional repression is linked to the open conformation of viral DNA in replication
302 compartments, and that this helps these viruses counteract decay-induced viral transcript loss.
303 While widespread mRNA decay has been shown to facilitate immune evasion, gene expression
304 control, and latency establishment, the robust viral transcription we document here presents a
305 parsimonious explanation for a novel way in which the virus benefits from accelerated decay.
306
307

308 ## Materials and Methods

309 **Plasmids and Primers**

310 pCDEF3 muSOX and VHS and SOX have been previously published (24). pCDEF3-GFP
311 was used as a control.

312 Primers used for qPCR and for cloning are listed in S2 Table. M7, M4 and CMV-puro were
313 made by cloning the respective promoter sequence upstream of the puromycin cassette in a
314 pLKO-sgRNA vector. The promoter of M4 was defined as the 1131bp upstream of the M4
315 coding region not overlapping with other viral ORFs and the promoter sequence of M7 was
316 previously published (46). pGL3-kLANA-puromycin was made by introducing the puromycin
317 gene into the I-CeuI and XbaI sites of pGL3-kLANA via InFusion (Clonetech) cloning. pGL3-
318 kLANA was made by amplifying KSHV's LANA promoter sequence (47) and using InFusion
319 cloning to introduce it into the XhoI and HindIII sites of pGL3.
320

321 **Cells and transfections**

322 MC57G mouse fibroblast cells (ATCC), 293T cells (ATCC) and NIH 3T3 cells (ATCC)
323 were maintained in DMEM (Invitrogen) supplemented with 10% fetal bovine serum (FBS).
324 iSLK BAC16 cells (48) were maintained in DMEM supplemented with 10% FBS and 1 mg/mL
325 hygromycin B. To reactivate iSLK cells, they were treated with 1 μg/mL doxycycline and 1 mM
326 sodium butyrate for 48 hours.
327 DNA transfections were carried out in 293T cells at 70-90% confluency in 10 cm plates
328 with 10 μg host-shutoff factor plasmid or vector control using PolyJet (SignaGen) 24 hours
329 before harvesting and again at 18 hours before harvesting.
330 Lentiviral transduction was carried out by spinfecting $1x10^6$ 293T or MC57G cells with
331 lentivirus made from 2nd generation plasmids at a MOI <1 for 2 hours with 4 μg/mL polybrene
332 (Fisher). Twenty-four hours later puromycin (1 μg/ml for 293T or 3 μg/ml for MC57G) was
333 added to select for transduced cells. 293T cells stably expressing the kLANA-puromycin cassette
334 were made by transfecting the cells with 1 μg pGL3-kLANA-puromycin using PolyJet, then
335 selecting with puromycin for random integration events.
336 For the CMV-luciferase promoter assay, populations of 293T cells expressing muSOX
337 were selected 24 hours post-transfection using the Miltenyi Biotec MACS cell separation system
338 according to the manufacturer's instructions as previously described (22).
339 293T cells were infected with KSHV by reactivating iSLK-Bac16 cells for 48 hours and
340 then spinfecting cell-free virus onto a monolayer of 293T cells, as described for lentiviral
341 production but in the absence of polybrene.
342 3 million MC57G cells were nucleofected with a 100uL Neon tip (1400 Voltage/20
343 Width/2 Pulse) to knockdown Xrn1 using a pool of 4 siRNAs (Dharmacon M-046621-01) or a
344 non-targeting control (Dharmacon D-001206-14) using 10 μL of 20 μM siRNA.

345

346 **4SU labeling**

347 Adapted from (49).Cells were incubated in suspension with 500 μM 4SU (Sigma T4509)
348 in DMEM supplemented with 10% FBS for 10 min then washed with PBS. RNA was extracted
349 with TRIzol followed by isopropanol purification. RNA (300 μg) was incubated in biotinylation
350 buffer (50 mM HEPES [pH 7.5], 5 mM EDTA) and 5 μg MTSEA-biotin (Biotium #90066),
351 rotating at room temperature in the dark for 30 min. A no biotin control was made from an equal
352 amount of total RNA and incubated as above but without the addition of MTSEA-biotin. RNA
353 was then phenol:chloroform extracted and precipitated with isopropanol. The pellet was
354 resuspended in DEPC-treated water and mixed with 50 μL Dynabeads MyOne streptavidin C1
355 (Invitrogen) that had been pre-washed twice with wash buffer (100 mM Tris [pH 7.5], 10 mM
356 EDTA, 1 M NaCl, 0.1% Tween 20). Samples were rotated in the dark for 1 hour at room
357 temperature, then washed twice with 65°C wash buffer and twice with room temperature wash
358 buffer. Samples were eluted twice with 100 μL 5% Beta-mercaptoethanol (BME) in DEPC H_20
359 for 5 min then RNA was precipitated with isopropanol and quantified by RT-qPCR.

360 **Viral mutagenesis, propagation and infections**

361 The WT and R443I MHV68 bacterial artificial chromosome (BAC) were previously
362 described (6,50). MHV68 was produced by first making p0 virus by transfecting NIH 3T3 cells
363 in 6-well plates with 2.5 μg BAC DNA using TransIT-X2 (Mirus Bio) for 24h. Five to seven
364 days later, the cells were split into a 10 cm dish, then harvested and frozen. After 5-7 days the
365 majority of cells showed cytopathic effect (CPE). 30 μL of p0 was then added per confluent 10
366 cm dish of NIH 3T12 cells, split 2 days later into four 10 cm dishes and harvested 4-6 days later
367 when all cells were infected. Cells were collected by centrifugation (5 min, 1500 rpm) and the

368 pellet was dounced 10 times. The cell pellet and supernatant were then ultracentrifuged for 2 h at
369 30,000 rpm. The resulting pellet was resuspended and titered by plaque assay. Cells were
370 infected with MHV68 at an MOI of 5 for 24 hours.
371
372 **Western blotting**
373 Cells were lysed in RIPA buffer (50 mM Tris-HCl pH7.6, 150 mM NaCl, 3 mM $MgCl_2$,
374 10% glycerol, 0.5% NP-40, cOmplete EDTA-free Protease Inhibitors [Roche]) and then clarified
375 by centrifugation at 21,000 x g for 10 min at 4˚C. Whole cell lysate was quantified by Bradford
376 assay and resolved by SDS-PAGE. Antibodies for western blot are: Xrn1 (Bethyl A300-443A,
377 1:1000), and Gapdh (Abcam, ab8245, 1:2000).
378
379 **RT-qPCR**
380 RNA was reverse transcribed using AMV RT (Promega) with random 9-mer primers.
381 Total RNA was DNase treated with TURBO DNase (ThermoFisher) or DNase treated on column
382 with Zymo Direct-zol RNA MiniPrep Plus DNase. cDNA was quantified using iTaq Universal
383 SYBR Mastermix (BioRad) and transcript-specific primers. All qPCR results are normalized to
384 18S levels and WT or vector control set to 1.
385
386 **Immunofluoresence**
387 NIH 3T3 cells were plated on coverslips (7.5 x 10^4 cells/well of a 12-well), infected the
388 following day for 25-27 h, and then fixed in 4% formaldehyde for 10 min. iSLK-Bac16 cells
389 were plated on coverslips (5 x 10^4 cells/well of a 12-well), reactivated 24h later with doxycycline
390 and sodium butyrate for 48 hours and then fixed as above. Cells were permeabilized with ice-

391 cold methanol at -20°C for at least 20 min and incubated with anti-Pol II antibody (Biolegend,
392 8WG16 at 1:200), anti-PABPC antibody (Abcam ab21060 at 1:200 for mouse cells and Santa
393 Cruz sc32318 at 1:25 for human cells) or anti-ORF59 antibody (Advanced Biotechnologies 13-
394 211-100 at 1:200) in 5% BSA overnight at 4 °C. Secondary antibodies were added (1:1000) for 1
395 h at 37 °C. Coverslips were mounted in DAPI- containing Vectashield (VectorLabs). We
396 identified RCs by DAPI exclusion and Pol II recruitment or ORF59 staining (28,30,51). Images
397 were collected on a Zeiss LSM 710 AxioObserver with a 40x oil objective. Cells with RCs were
398 first identified, then PABPC co-localization was determined by counting cells with at least 2x
399 nuclear pixel intensity relative to non-RC containing cells in the same image (ImageJ).
400

401 **Chromatin immunoprecipitation (ChIP)**

402 ChIP was performed from 15 cm plates of cells. 3 x 10^6 MC57G or 293T cells were
403 plated 24 h before infection and then harvested 24 h after infection or transfection(s). Upon
404 harvesting, cells were washed with PBS, crosslinked in 1% formaldehyde at room temperature
405 for 10 min. Cells were quenched in 0.125 M glycine for 5 min and washed twice with cold PBS.
406 Crosslinked cell pellets were mixed with 1 mL fractionation buffer (5mM PIPES pH 8.0, 85 mM
407 KCl, 0.5% NP-40 with cOmplete EDTA-free Protease Inhibitors [Roche]) and incubated on ice
408 for 10 min, during which time the lysate was dounce homogenized to release nuclei and spun at
409 4,000 rpm for 5 min at 4°C to pellet nuclei. Nuclei were then resuspended in 300 µl of nuclei
410 lysis buffer (50mM Tris-HCl pH 8.0, 0.3% SDS, 10mM EDTA, with cOmplete EDTA-free
411 Protease Inhibitors [Roche]) and rotated for 10 min at 4°C followed by sonication using a
412 QSonica Ultrasonicator. Sonicated chromatin was then spun at 13,000 rpm for 10 min at 4°C and
413 the pellet discarded. 40 µg of chromatin measured with the Qubit broad range DNA reagent

414 (ThermoFisher) was brought to 500 µL with ChIP dilution buffer (16.7 mM Tris-HCl pH 8.0,
415 1.1% Triton X-100, 1.2 mM EDTA, 167 mM NaCl and cOmplete EDTA-free Protease Inhibitors
416 [Roche]) and incubated with 10 µg mouse monoclonal anti-RNAPII (BioLegend, 8WG16) or
417 mouse IgG (Fisher Scientific) overnight, whereupon samples were rotated with 20 µl protein G
418 dynabeads (Thermofisher) for 2 hours at 4°C. Beads were washed with low salt immune complex
419 (20 mM Tris pH 8.0, 1% Triton-x-100, 2 mM EDTA, 150 mM NaCl, 0.1% SDS), high salt
420 immune complex (20 mM Tris pH 8.0, 1% Triton-x-100, 2 mM EDTA, 500 mM NaCl, 0.1%
421 SDS), lithium chloride immune complex (10 mM Tris pH 8.0, 0.25 M LiCl, 1% NP-40, 1%
422 Deoxycholic acid, 1 mM EDTA), and Tris-EDTA for 5 min each at 4°C with rotation. DNA was
423 eluted from the beads using 100 µl of elution buffer (150 mM NaCl, 50 µg/ml Proteinase K) and
424 incubated at 55°C for 2 hours, then 65°C for 12 hours. DNA was purified using a Zymo Oligo
425 Clean & Concentrator kit, and quantified by qPCR using primers to the promoter regions of
426 indicated genes for 50 cycles. qPCR was simultaneously performed on input chromatin and
427 normalized to input. Raw percent input values are normalized by setting mock infected or a
428 transfection control to 1 and are plotted as relative % input. IgG pull downs were performed with
429 the MHV68 infected sample under scramble conditions, or the muSOX or SOX transfected
430 sample for transfection experiments.
431
432 **ChIP Sequencing and data analysis**
433 Libraries were prepared for sequencing (Kapa Hyper Prep) using equal amounts of
434 chromatin within each experiment, amplified for 10-12 cycles based on Kapa's recommendations
435 and sequenced on a HiSeq4000 with 100bp single end reads or 150bp reads (Xrn1kd second
436 replicate only). Sequencing quality was assessed with FastQC and trimmed with Sickle. A

437 custom index was made of the mm10 and MHV68 genomes with Bowtie2 build. Reads were
438 mapped to that index using Bowtie2 (2.3.0).
439 To visualize reads in the Integrative Genomics Viewer (IGV), tdf files were made from
440 bam files and indexes made from those bam files. To make tdf files for the viral genome, a
441 chrom.size file was created for MHV68 and then the count command was run. Analysis of
442 mapped reads was performed with HOMER (Hypergeometric Optimization of Motif
443 EnRichment) (52). Tag directories were created from the bam files generated from Bowtie with
444 the makeTagDirectory command. This was done separately for the mouse and MHV68 genomes.
445 For mouse genes, the analyzeRepeats command was used to look at tag density in the body of
446 genes and the –c pausing option was used to compare pausing ratios. annotatePeaks was run in
447 both the –hist and –ghist mode to assess composite Pol II occupancy across the mouse genome as
448 well as individual gene occupancy.
449 Viral analyses were done by first creating a custom genome annotation in HOMER using
450 the loadGenome command. The TSS file was created from data generously shared by Scott
451 Tibbetts (University of Florida) including portions of the viral BAC provided by Laurie Krug
452 (Stony Brook University). annotatePeaks was run in the –hist mode to assess composite Pol II
453 occupancy across the viral genome as well as individual gene occupancy.
454

455 **Acknowledgements**

456 We thank all members of the Glaunsinger and Coscoy labs for their helpful suggestions and
457 discussions. We thank David McSwiggen for his microscopy assistance, Jennifer Kugel for her
458 guidance applying HOMER to the viral genome, Scott Tibbetts for sharing MHV68 TSS data and

459 Laurie Krug for providing a KSHV BAC sequence. This work used the Vincent J. Coates
460 Genomics Sequencing Laboratory at UC Berkeley.
461

462 ## Figure Legends

463 **Fig 1: Promoter-proximal Pol II recruitment to mammalian genes is RNA-decay dependent**
464 (A) Pol II ChIP-seq signal profiles of host genes in mock-infected, MHV68-infected and R443I-
465 infected MC57G cells. Each row of the heat map displays Pol II occupancy of one gene from -
466 1000 to +1000 in 25 bp bins. Genes are ranked by the Pol II-transcription start site (TSS)
467 proximal signal in mock infected cells. (B) ChIP-qPCR validation of Pol II occupancy at the
468 *Rplp0* and *Fus* promoters. Pol II ChIP was performed on mock, MHV68 WT or MHV68 R443I
469 infected MC57G cells and Pol II levels were assayed near the TSS of two repressed host genes
470 during MHV68 infection from the ChIP-seq data. (* $p < 0.05$, ** $p < 0.01$, students t-test) (C)
471 Sequence tags were plotted as a histogram with 25 bp bins for -2000 to +4000 around the TSS.
472 Mock (red), MHV68 (blue) and MHV68 R443I (green) traces are shown along with their input
473 controls. (D) Scatterplot of Pol II occupancy of promoters, averaging the sum of ChIP-seq tags
474 from -50 to +200 across two replicate experiments with inputs subtracted out. Mock is compared
475 to WT MHV68 infection on the left and to MHV68 R443I infection on the right. Linear
476 regression lines are plotted in blue and equations are provided. A y=x line is plotted for reference
477 in red. (E) Scatterplot of Pol II occupancy of gene bodies, averaging the sum of ChIP-seq tags
478 from -50 to +200 across two replicate experiments with inputs subtracted out. Data as described
479 for (D) (E) Pol II transcription termination is not dependent on RNA decay. Sequence tags were
480 plotted as a histogram in 25 bp bins for transcription termination sequence (TTS) proximal Pol II
481 for -1000 to +1000 around the TTS with the same color scheme as (C).

482 **Fig 2: Viral genes are not susceptible to RNA decay dependent Pol II repression**

483 (A) Viral gene Pol II recruitment is independent of RNA decay. Sequence tags were plotted as a
484 histogram in 25 bp bins for -500 to +500 around the TSS. MHV68 WT (blue) and R443I (green)
485 traces are shown from infected MC57G cells. (B) Pol II ChIP-seq coverage across 5.5 kb of the
486 MHV68 genome for MHV68 WT and R443I in wild type (WT) cells and MHV68 infection in
487 Xrn1 kd cells. Alignment files were converted to tdf format and visualized in the IGV. (C) Pol II
488 ChIP qPCR signal is similar across gene bodies. Three regions of the ORF54 and ORF37 gene
489 were assayed by Pol II ChIP-qPCR during MHV68 WT or R443I infection to assess the relative
490 levels of Pol II across the gene.

491

492 **Fig 2: PABPC is not excluded from replication compartments**

493 (A) Imunofluoresence (IF) was performed on MHV68 infected 3T3 cells at 27 hpi and stained
494 with PABPC, Pol II and DAPI. The MHV68 genome contains GFP, which served as a marker of
495 infection. Cells with RCs are denoted with red arrows. RCs were identified in cell nuclei with
496 PolII staining overlapping regions that are DAPI negative. The inset shows a merge of Pol II and
497 PABPC staining for several cells that co-stain for both proteins in RCs. (B) IF was performed on
498 KSHV-positive iSLK cells reactivated for 48 h and stained with antibodies against PABPC,
499 ORF59 and DAPI. Cells with RCs are denoted with arrows and were identified in cell nuclei
500 with ORF59 staining that overlaps with DAPI negative regions. The inset shows a merge of
501 ORF59 and PABPC staining for several cells that co-stain for both proteins in RCs. (C) Percent
502 of RC containing cells that overlap with PABPC signal. Fractions of cells with PABPC signal in
503 RCs over total number of cells counted with RCs are displayed.

504

505 **Fig 3: Viral promoter sequences are insufficient to escape transcriptional regulation**

506 (A) The MHV68 M7 viral promoter driving puromycin resistance was lentivirally integrated
507 into 293T cells. 24 h post transfection of muSOX or VHS, Pol II-ChIP qPCR was used to
508 measure Pol II levels at two host promoters (*Gapdh*, *Rplp0*) and the integrated M7 promoter. (* p
509 < 0.05, ** p < 0.01, *** p <0.001, **** p<0.0001 students t-test) (B) The KSHV LANA
510 promoter driving puromycin resistance was integrated into 293T cells by random incorporation.
511 Pol II-ChIP qPCR was used to measure Pol II levels 24 h post SOX or VHS transfection as
512 described above. (C) The MHV68 M4 viral promoter driving puromycin resistance was
513 lentivirally integrated into MC57G cells. The cells were then infected with WT MHV68 or
514 R443I at a MOI of 5 and Pol II levels at the indicated promoters were assayed by Pol II ChIP-
515 qPCR.

516

517 **Fig 4: Non-MHV68 promoters escape repression on the viral genome**

518 (A) 4SU incorporated RNA levels of luciferase driven by CMV in muSOX and vector-control
519 expressing 293T cells. Cells were separated using the co-expressed Thy1.1 marker to ensure pure
520 populations of transfected cells(22). (B) The CMV promoter driving puromycin resistance was
521 lentivirally integrated into MC57G cells. The cells were then infected with WT MHV68 or
522 R443I at an MOI of 5 and Pol II levels at the indicated promoters were assayed by Pol II ChIP-
523 qPCR. (C) ChIP-seq traces comparing WT MHV68 to R443I coverage from -300 to +200 around
524 the TSS in 25 bp bins, averaged from two biological replicates of infected MC57G cells. Six
525 representative viral genes and CMV-GFP are shown. (D) 293T cells were infected with KSHV
526 and then transfected with muSOX twice over a 24 h period to induce accelerated decay. Pol II

527 levels at the indicated KSHV and human promoters were measured by ChIP-qPCR. (** $p < 0.01$,
528 students t-test)
529

530 ## Supporting information

531

532 **S1 Fig ChIP-seq replicate with WT and R443I MHV68**

533 A) Pol II ChIP-seq signal profiles of host genes are shown in mock-infected, MHV68-infected
534 and R443I-infected cells. Each row of the heat map displays Pol II occupancy of one gene from -
535 1000 to +1000 in 25 bp bins. Genes are ranked by the Pol II-transcription start site (TSS)
536 proximal signal in mock infected cells. (B) Sequence tags were plotted as a histogram in 25 bp
537 bins for -2000 to +4000 around the TSS. Mock, MHV68 (red) and MHV68 (blue) and R443I
538 (green) traces are shown along with their input controls. (C) Pol II ChIP-seq coverage across the
539 *Srsf2* gene for ChIP-seq replicate 1 and 2 with mock, WT MHV68 and R443I shown. Alignment
540 files were converted to the tiled data file (tdf) format and visualized in the Integrative Genome
541 Viewer. (D) Pol II transcription termination is not dependent on RNA decay. Sequence tags were
542 plotted as a histogram in 25 bp bins for transcription termination sequence (TTS) proximal Pol II
543 for -1000 to +1000 around the TTS with the same color scheme as (B).
544

545 **S2 Fig Unreactivated iSLK cells show primarily cytoplasmic PABPC signal**

546 (A)IF was performed on unreactivated iSLK cells using antibodies recognizing PABPC and
547 ORF59. Host DNA was stained with DAPI.
548

549 S3? Fig 4SU-enriched RNA from MHV68 and R443I infected MC57G cells

550 (A) 4SU incorporated RNA levels of 7 viral genes in cells infected with MHV68 and R443I.

551
552
553 **References**
554

555 1. Sun M, Schwalb B, Schulz D, Pirkl N, Etzold S, Lariviere L, et al. Comparative dynamic
556 transcriptome analysis (cDTA) reveals mutual feedback between mRNA synthesis and
557 degradation. Genome Research. 2012 Jul 2;22(7):1350–9.

558 2. Haimovich G, Medina DA, Causse SZ, Garber M, Millán-Zambrano G, Barkai O, et al.
559 Gene Expression Is Circular: Factors for mRNA Degradation Also Foster mRNA
560 Synthesis. Cell. Elsevier Inc; 2013 May 23;153(5):1000–11.

561 3. Shalem O, Dahan O, Levo M, Martinez MR, Furman I, Segal E, et al. Transient
562 transcriptional responses to stress are generated by opposing effects of mRNA production
563 and degradation. Mol Syst Biol. EMBO Press; 2008;4(1):223–10.

564 4. Shalem O, Groisman B, Choder M, Dahan O, Pilpel Y. Transcriptome Kinetics Is
565 Governed by a Genome-Wide Coupling of mRNA Production and Degradation: A Role
566 for RNA Pol II. Barsh GS, editor. PLoS Genet. Public Library of Science; 2011 Sep
567 8;7(9):e1002273–10.

568 5. Dori-Bachash M, Shalem O, Manor YS, Pilpel Y, Tirosh I. Widespread promoter-
569 mediated coordination of transcription and mRNA degradation. Genome Biol. BioMed
570 Central; 2012;13(12).

571 6. Richner JM, Clyde K, Pezda AC, Cheng BYH, Wang T, Kumar GR, et al. Global mRNA
572 Degradation during Lytic Gammaherpesvirus Infection Contributes to Establishment of
573 Viral Latency. Speck SH, editor. PLoS Pathog. 2011 Jul 21;7(7):e1002150–13.

574 7. Liu SW, Wyatt LS, Orandle MS, Minai M, Moss B. The D10 Decapping Enzyme of
575 Vaccinia Virus Contributes to Decay of Cellular and Viral mRNAs and to Virulence in
576 Mice. Journal of Virology. 6 ed. 2013 Dec 18;88(1):202–11.

577 8. Parrish S, Moss B. Characterization of a vaccinia virus mutant with a deletion of the
578 D10R gene encoding a putative negative regulator of gene expression. Journal of
579 Virology. American Society for Microbiology; 2006 Jan;80(2):553–61.

580 9. Read GS. Virus-encoded endonucleases: expected and novel functions. WIREs RNA. 1st
581 ed. 2013 Jul 30;4(6):693–708.

582 10. Dauber B, Poon D, Santos dos T, Duguay BA, Mehta N, Saffran HA, et al. The Herpes
583 Simplex Virus Virion Host Shutoff Protein Enhances Translation of Viral True Late
584 mRNAs Independently of Suppressing Protein Kinase R and Stress Granule Formation.
585 Sandri-Goldin RM, editor. Journal of Virology. 2016 Jun 10;90(13):6049–57.

586 11. Karr BM, Read GS. The virion host shutoff function of herpes simplex virus degrades the
587 5“ end of a target mRNA before the 3” end. Virology. 1999 Nov 10;264(1):195–204.

588 12. Glaunsinger B, Chavez L, Ganem D. The Exonuclease and Host Shutoff Functions of the
589 SOX Protein of Kaposi's Sarcoma-Associated Herpesvirus Are Genetically Separable.
590 Journal of Virology. 2005 May 26;79(12):7396–401.

591 13. Huang C, Lokugamage KG, Rozovics JM, Narayanan K, Semler BL, Makino S. SARS
592 Coronavirus nsp1 Protein Induces Template-Dependent Endonucleolytic Cleavage of
593 mRNAs: Viral mRNAs Are Resistant to nsp1-Induced RNA Cleavage. Baric RS, editor.
594 PLoS Pathog. 2011 Dec 8;7(12):e1002433–18.

595 14. Kamitani W, Huang C, Narayanan K, Lokugamage KG, Makino S. A two-pronged
596 strategy to suppress host protein synthesis by SARS coronavirus Nsp1 protein. Nature
597 Structural & Molecular Biology. Nature Publishing Group; 2009 Oct 18;16(11):1134–40.

598 15. Jagger BW, Wise HM, Kash JC, Walters K-A, Wills NM, Xiao Y-L, et al. An
599 Overlapping Protein-Coding Region in Influenza A Virus Segment 3 Modulates the Host
600 Response. Science. 2012;337(6091):199–204.

601 16. Covarrubias S, Gaglia MM, Kumar GR, Wong W, Jackson AO, Glaunsinger BA.
602 Coordinated Destruction of Cellular Messages in Translation Complexes by the
603 Gammaherpesvirus Host Shutoff Factor and the Mammalian Exonuclease Xrn1. Renne R,
604 editor. PLoS Pathog. 2011 Oct 27;7(10):e1002339–15.

605 17. Gaglia MM, Covarrubias S, Wong W, Glaunsinger BA. A Common Strategy for Host
606 RNA Degradation by Divergent Viruses. Journal of Virology. 2012 Aug 9;86(17):9527–
607 30.

608 18. Eckmann CR, Rammelt C, Wahle E. Control of poly(A) tail length. WIREs RNA. 2010
609 Nov 17;2(3):348–61.

610 19. Gallouzi IE, Wilusz J. A DIStinctively novel exoribonuclease that really likes U. EMBO
611 J. Nature Publishing Group; 2013 Jun 11;32(13):1799–801.

612 20. Schoenberg DR, Maquat LE. Re-capping the message. Trends in Biochemical Sciences.
613 2009 Sep;34(9):435–42.

614 21. Abernathy E, Glaunsinger B. Emerging roles for RNA degradation in viral replication and
615 antiviral defense. Virology. Elsevier; 2015 May 1;479-480(C):600–8.

616 22. Gilbertson S, Federspiel JD, Hartenian E, eLife IC, 2018. Changes in mRNA abundance
617 drive shuttling of RNA binding proteins, linking cytoplasmic RNA degradation to
618 transcription. eLife.

619 23. Abernathy E, Clyde K, Yeasmin R, Krug LT, Burlingame A, Coscoy L, et al.
620 Gammaherpesviral Gene Expression and Virion Composition Are Broadly Controlled by

621 Accelerated mRNA Degradation. van Dyk LF, editor. PLoS Pathog. 2014 Jan
622 16;10(1):e1003882–14.

623 24. Abernathy E, Gilbertson S, Alla R, Glaunsinger B. Viral Nucleases Induce an mRNA
624 Degradation- Transcription Feedback Loop in Mammalian Cells. Cell Host Microbe.
625 Elsevier Inc; 2015 Jul 21;18(2):1–12.

626 25. Chang L, Godinez WJ, Kim, I, 2011. Herpesviral replication compartments move and
627 coalesce at nuclear speckles to enhance export of viral late mRNA. Proceedings of the
628 National Academy of Sciences. 2011 May;108(21):E136-E144.

629 26. Taylor TJ, McNamee EE, Day C, Knipe DM. Herpes simplex virus replication
630 compartments can form by coalescence of smaller compartments. Virology. 2003
631 May;309(2):232–47.

632 27. Monier K, Armas JCG, Etteldorf S, Ghazal P, Sullivan KF. Annexation of the
633 interchromosomal space during viral infection. Nat Cell Biol. Nature Publishing Group;
634 2000 Sep 1;2(9):661–5.

635 28. Li D, Fu W, Swaminathan S. Continuous DNA replication is required for late gene
636 transcription and maintenance of replication compartments in gammaherpesviruses.
637 Robertson ES, editor. PLoS Pathog. 2018 May 29;14(5):e1007070–25.

638 29. Dembowski JA, DeLuca NA. Selective Recruitment of Nuclear Factors to Productively
639 Replicating Herpes Simplex Virus Genomes. Everett RD, editor. PLoS Pathog. 2015 May
640 27;11(5):e1004939–35.

641 30. Rice SA, Long MC, LAM V, Spencer CA. Rna-Polymerase-Ii Is Aberrantly
642 Phosphorylated and Localized to Viral Replication Compartments Following Herpes-
643 Simplex Virus-Infection. Journal of Virology. American Society for Microbiology
644 (ASM); 1994 Feb;68(2):988–1001.

645 31. Kumar GR, Shum L, Glaunsinger BA. Importin alpha-mediated nuclear import of
646 cytoplasmic poly(A) binding protein occurs as a direct consequence of cytoplasmic
647 mRNA depletion. Molecular and Cellular Biology. American Society for Microbiology;
648 2011 Aug;31(15):3113–25.

649 32. Darzacq X, Shav-Tal Y, de Turris V, Brody Y, Shenoy SM, Phair RD, et al. In vivo
650 dynamics of RNA polymerase II transcription. Nat Struct Mol Biol. 2007 Aug
651 5;14(9):796–806.

652 33. Nojima T, Gomes T, Grosso ARF, Kimura H, Dye MJ, Dhir S, et al. Mammalian NET-
653 Seq Reveals Genome-wide Nascent Transcription Coupled to RNA Processing. Cell. The
654 Authors; 2015 Apr 23;161(3):526–40.

655 34. Rutkowski AJ, Erhard F, L'Hernault A, Bonfert T, Schilhabel M, Crump C, et al.
656 Widespread disruption of host transcription termination in HSV-1 infection. Nature
657 Communications. 2015;6:7126.

658 35. Abrisch RG, Eidem TM, Yakovchuk P, Kugel JF, Goodrich JA. Infection by Herpes
659 Simplex Virus 1 Causes Near-Complete Loss of RNA Polymerase II Occupancy on the
660 Host Cell Genome. Sandri-Goldin RM, editor. Journal of Virology. American Society for
661 Microbiology; 2016 Mar;90(5):2503–13.

662 36. Spencer CA, Dahmus ME, Rice SA. Repression of host RNA polymerase II transcription
663 by herpes simplex virus type 1. Journal of Virology. 1997 Mar;71(3):2031–40.

664 37. Smiley JR, Smibert C, Everett RD. Expression of a Cellular Gene Cloned in Herpes-
665 Simplex Virus - Rabbit Beta-Globin Is Regulated as an Early Viral Gene in Infected
666 Fibroblasts. Journal of Virology. American Society for Microbiology (ASM); 1987
667 Aug;61(8):2368–77.

668 38. Smibert CA, Smiley JR. Differential Regulation of Endogenous and Transduced Beta-
669 Globin Genes During Infection of Erythroid-Cells with a Herpes-Simplex Virus Type-1
670 Recombinant. Journal of Virology. American Society for Microbiology Journals; 1990
671 Aug;64(8):3882–94.

672 39. Smiley JR. Herpes simplex virus virion host shutoff protein: immune evasion mediated by
673 a viral RNase? Journal of Virology. American Society for Microbiology Journals; 2004
674 Feb;78(3):1063–8.

675 40. Schmid M, Speiseder T, Dobner T, Gonzalez RA. DNA Virus Replication Compartments.
676 Journal of Virology. 4 ed. 2014 Jan 14;88(3):1404–20.

677 41. Günther T, Grundhoff A. The Epigenetic Landscape of Latent Kaposi Sarcoma-
678 Associated Herpesvirus Genomes. Kellam P, editor. PLoS Pathog. 2010 Jun
679 3;6(6):e1000935–19.

680 42. Szyf M, Eliasson L, Mann V, Klein G, Razin A. Cellular and Viral-Dna Hypomethylation
681 Associated with Induction of Epstein-Barr Virus Lytic Cycle. Proc Natl Acad Sci USA.
682 National Academy of Sciences; 1985;82(23):8090–4.

683 43. Hilton IB, Simon JM, Lieb JD, Davis IJ, Damania B, Dittmer DP. The Open Chromatin
684 Landscape of Kaposi's Sarcoma-Associated Herpesvirus. Journal of Virology. 2013 Oct
685 3;87(21):11831–42.

686 44. Toth Z, Maglinte DT, Lee SH, Lee H-R, Wong L-Y, Brulois KF, et al. Epigenetic
687 Analysis of KSHV Latent and Lytic Genomes. Kellam P, editor. PLoS Pathog. Public
688 Library of Science; 2010 Jul 22;6(7):e1001013–7.

689 45. Hollingworth R, Horniblow RD, Forrest C, Stewart GS, Grand RJ. Localization of
690 Double-Strand Break Repair Proteins to Viral Replication Compartments following Lytic
691 Reactivation of Kaposi's Sarcoma-Associated Herpesvirus. Jung JU, editor. Journal of
692 Virology. 2017 Oct 27;91(22):1186–21.

693 46. Wong-Ho E, Wu TT, Davis ZH, Zhang B, Huang J, Gong H, et al. Unconventional
694 Sequence Requirement for Viral Late Gene Core Promoters of Murine Gammaherpesvirus
695 68. Journal of Virology. 2014 Feb 24;88(6):3411–22.

696 47. Jeong J, Papin J, Dittmer D. Differential Regulation of the Overlapping Kaposi's Sarcoma-
697 Associated Herpesvirus vGCR (orf74) and LANA (orf73) Promoters. Journal of Virology.
698 2001 Feb 15;75(4):1798–807.

699 48. Brulois KF, Chang H, Lee ASY, Ensser A, Wong LY, Toth Z, et al. Construction and
700 Manipulation of a New Kaposi's Sarcoma-Associated Herpesvirus Bacterial Artificial
701 Chromosome Clone. Journal of Virology. 2012 Aug 23;86(18):9708–20.

702 49. Duffy EE, Rutenberg-Schoenberg M, Stark CD, Kitchen RR, Gerstein MB, Simon MD.
703 Tracking Distinct RNA Populations Using Efficient and Reversible Covalent Chemistry.
704 Molecular Cell. 2015 Sep;59(5):858–66.

705 50. Adler H, Messerle M, Wagner M, Koszinowski UH. Cloning and mutagenesis of the
706 murine gammaherpesvirus 68 genome as an infectious bacterial artificial chromosome.
707 Journal of Virology. 2000 Aug;74(15):6964–74.

708 51. Dai-Ju JQ, Li L, Johnson LA, Sandri-Goldin RM. ICP27 Interacts with the C-Terminal
709 Domain of RNA Polymerase II and Facilitates Its Recruitment to Herpes Simplex Virus 1
710 Transcription Sites, Where It Undergoes Proteasomal Degradation during Infection.
711 Journal of Virology. 2006 Mar 14;80(7):3567–81.

712 52. Heinz S, Benner C, Spann N, Bertolino E, Lin YC, Laslo P, et al. Simple Combinations of
713 Lineage-Determining Transcription Factors Prime cis-Regulatory Elements Required for
714 Macrophage and B Cell Identities. Molecular Cell. Elsevier Inc; 2010 May 28;38(4):576–
715 89.

716

Figure 1

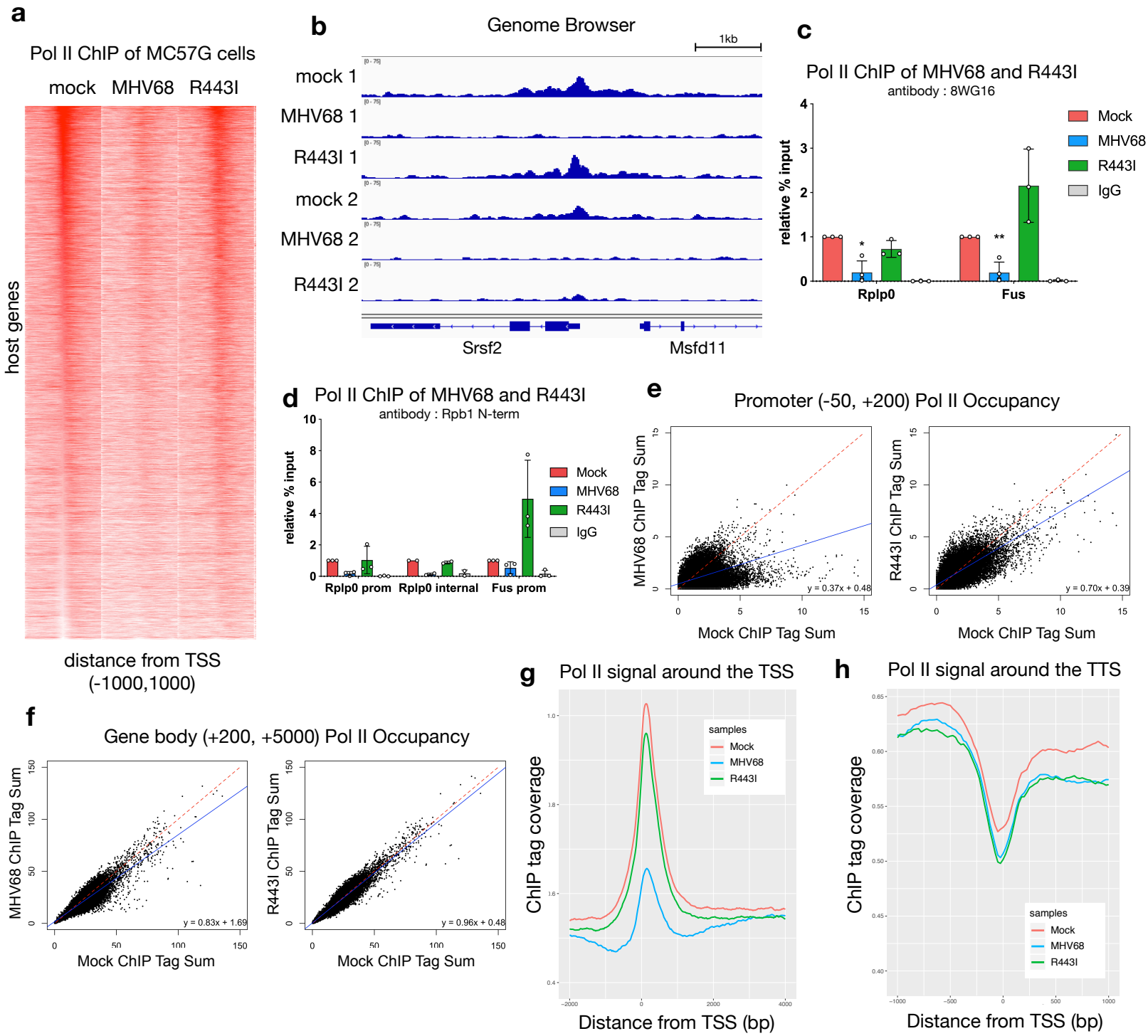
a
Pol II ChIP of MC57G cells
mock MHV68 R443I
host genes
distance from TSS
(-1000,1000)
b
Genome Browser
1kb
mock 1
MHV68 1
R443I 1
mock 2
MHV68 2
R443I 2
Srsf2
Msfd11
c
Pol II ChIP of MHV68 and R443I
antibody : 8WG16
relative % input
Mock
MHV68
R443I
IgG
Rplp0
Fus
d
Pol II ChIP of MHV68 and R443I
antibody : Rpb1 N-term
relative % input
Rplp0 prom
Rplp0 internal
Fus prom
e
Promoter (-50, +200) Pol II Occupancy
MHV68 ChIP Tag Sum
R443I ChIP Tag Sum
Mock ChIP Tag Sum
y = 0.37x + 0.48
y = 0.70x + 0.39
f
Gene body (+200, +5000) Pol II Occupancy
y = 0.83x + 1.69
y = 0.96x + 0.48
g
Pol II signal around the TSS
ChIP tag coverage
samples
Distance from TSS (bp)
h
Pol II signal around the TTS

Figure 2

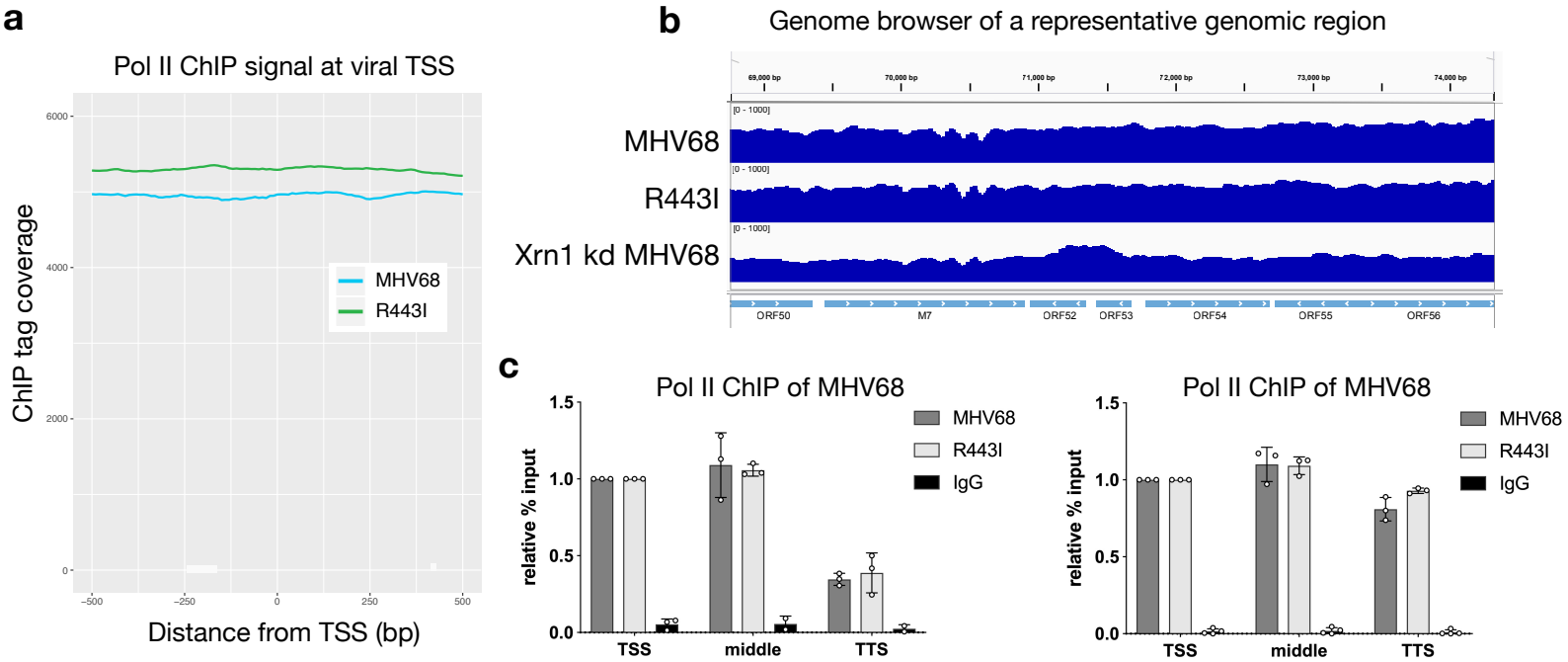
a
Pol II ChIP signal at viral TSS
ChIP tag coverage
6000
4000
2000
0
−500
−250
0
250
500
Distance from TSS (bp)
MHV68
R443I
b
Genome browser of a representative genomic region
69,000 bp
70,000 bp
71,000 bp
72,000 bp
73,000 bp
74,000 bp
MHV68
R443I
Xrn1 kd MHV68
[0 - 1000]
ORF50
M7
ORF52
ORF53
ORF54
ORF55
ORF56
c
Pol II ChIP of MHV68
relative % input
1.5
1.0
0.5
0.0
TSS
middle
TTS
MHV68
R443I
IgG
Pol II ChIP of MHV68
relative % input
1.5
1.0
0.5
0.0
TSS
middle
TTS
MHV68
R443I
IgG

Figure 3

a

MHV68 infection of 3T3s

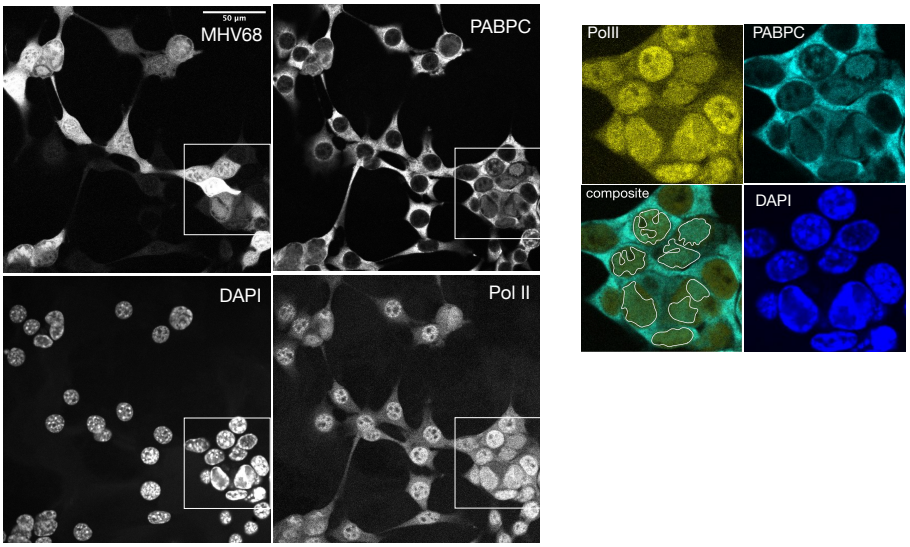

b

KSHV reactivation of iSLKs

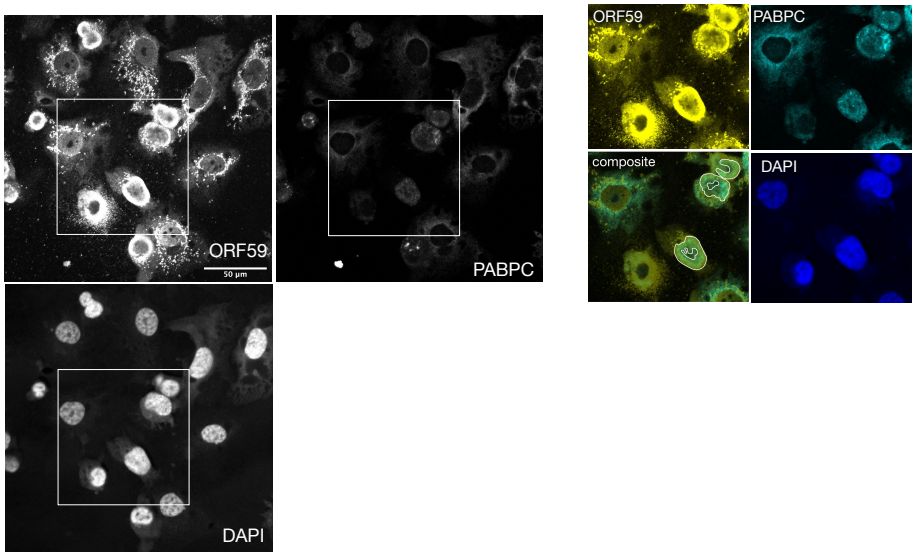

c

Percent of cells co-staining for PABPC and replication compartments

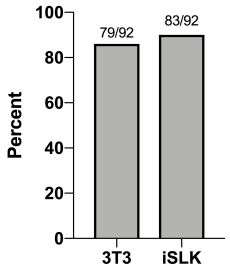

Figure 4

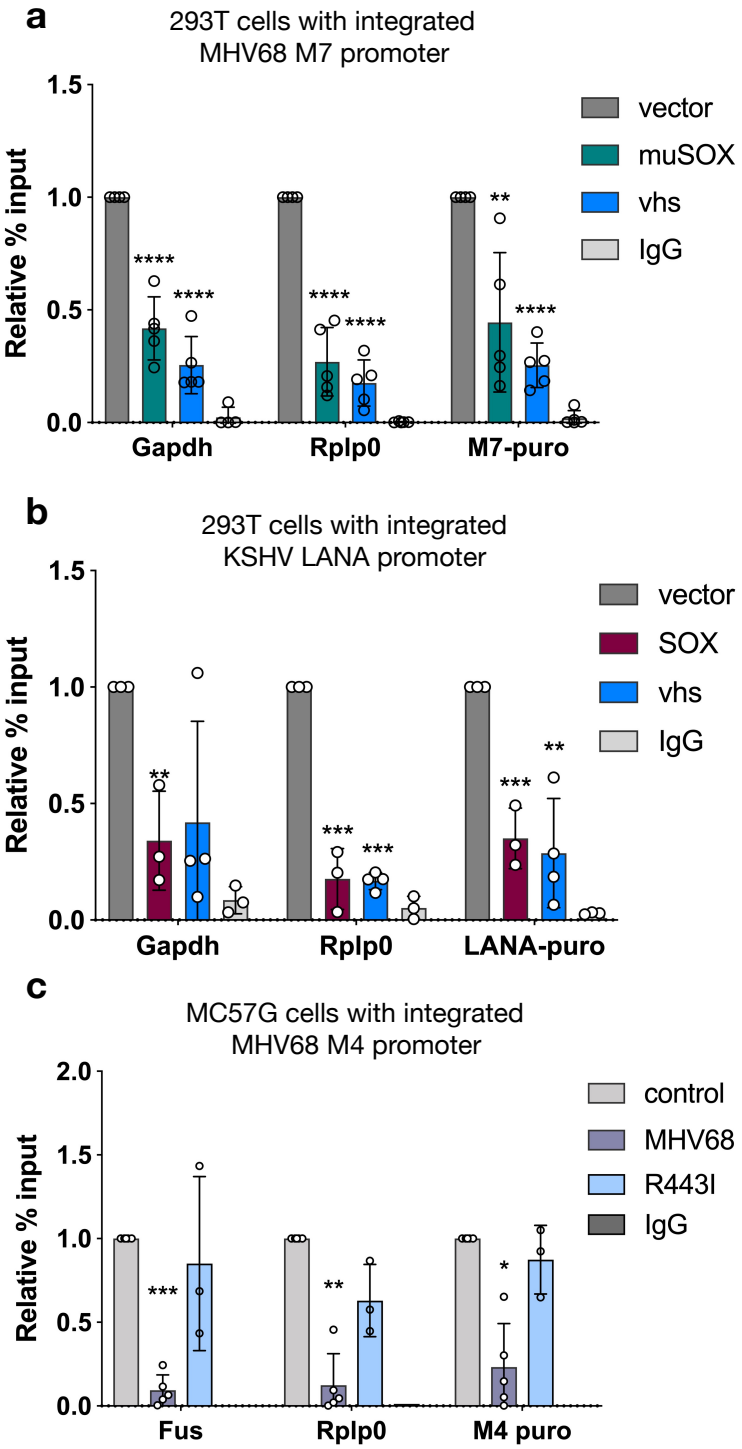
a
293T cells with integrated
MHV68 M7 promoter
Relative % input
1.5
1.0
0.5
0.0
vector
muSOX
vhs
IgG
****
****
****
****
**
****
Gapdh
Rplp0
M7-puro
b
293T cells with integrated
KSHV LANA promoter
Relative % input
1.5
1.0
0.5
0.0
vector
SOX
vhs
IgG
**
***
***
***
**
Gapdh
Rplp0
LANA-puro
c
MC57G cells with integrated
MHV68 M4 promoter
Relative % input
2.0
1.5
1.0
0.5
0.0
control
MHV68
R443I
IgG
***
**
*
Fus
Rplp0
M4 puro

Figure 5

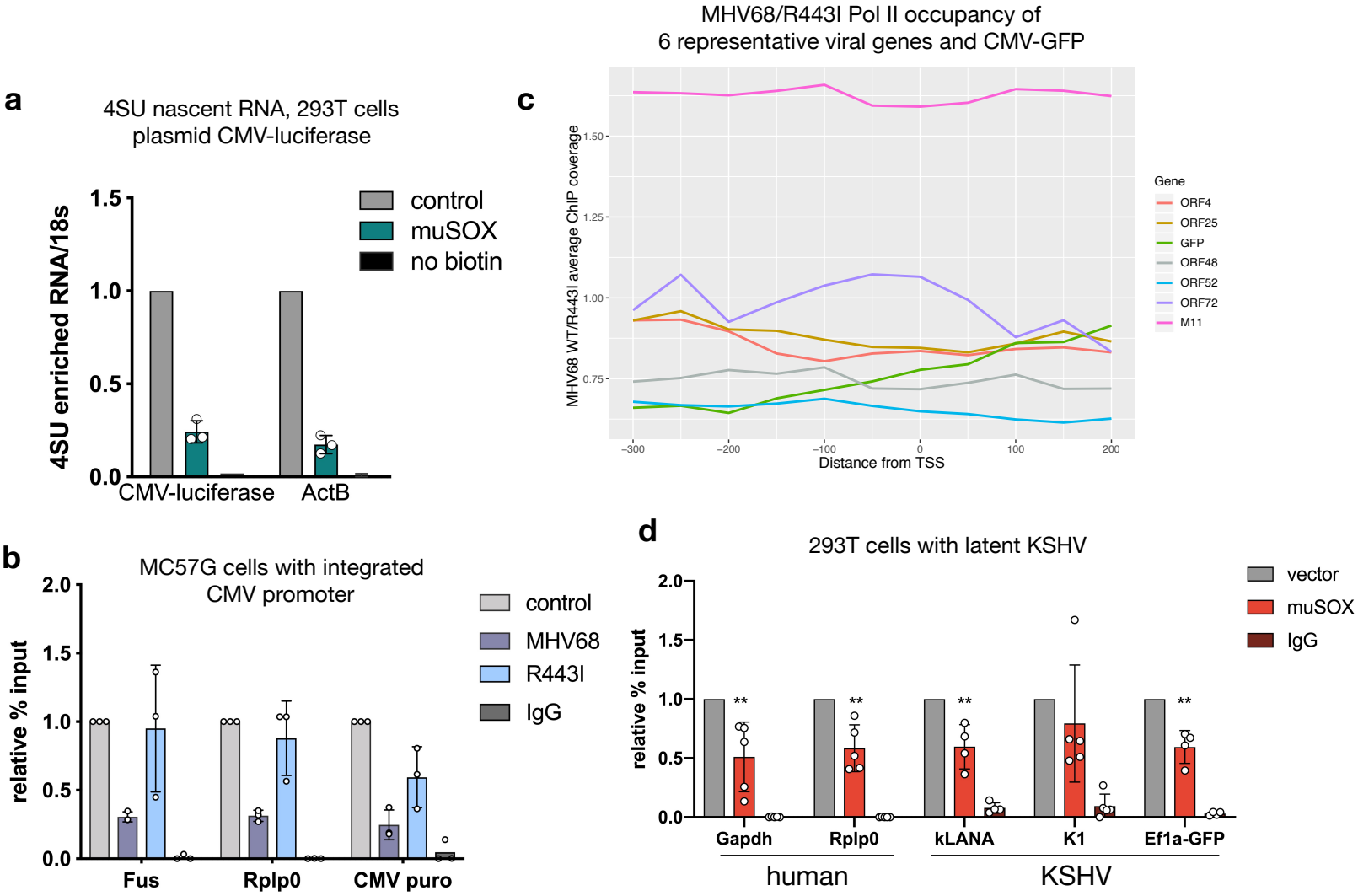
a
4SU nascent RNA, 293T cells
plasmid CMV-luciferase
4SU enriched RNA/18s
1.5
1.0
0.5
0.0
control
muSOX
no biotin
CMV-luciferase
ActB
b
MC57G cells with integrated
CMV promoter
relative % input
2.0
1.5
1.0
0.5
0.0
control
MHV68
R443I
IgG
Fus
Rplp0
CMV puro
c
MHV68/R443I Pol II occupancy of
6 representative viral genes and CMV-GFP
MHV68 WT/R443I average ChIP coverage
1.50
1.25
1.00
0.75
−300
−200
−100
0
100
200
Distance from TSS
Gene
ORF4
ORF25
GFP
ORF48
ORF52
ORF72
M11
d
293T cells with latent KSHV
relative % input
2.0
1.5
1.0
0.5
0.0
vector
muSOX
IgG
**
Gapdh
Rplp0
kLANA
K1
Ef1a-GFP
human
KSHV

Supp Figure 1

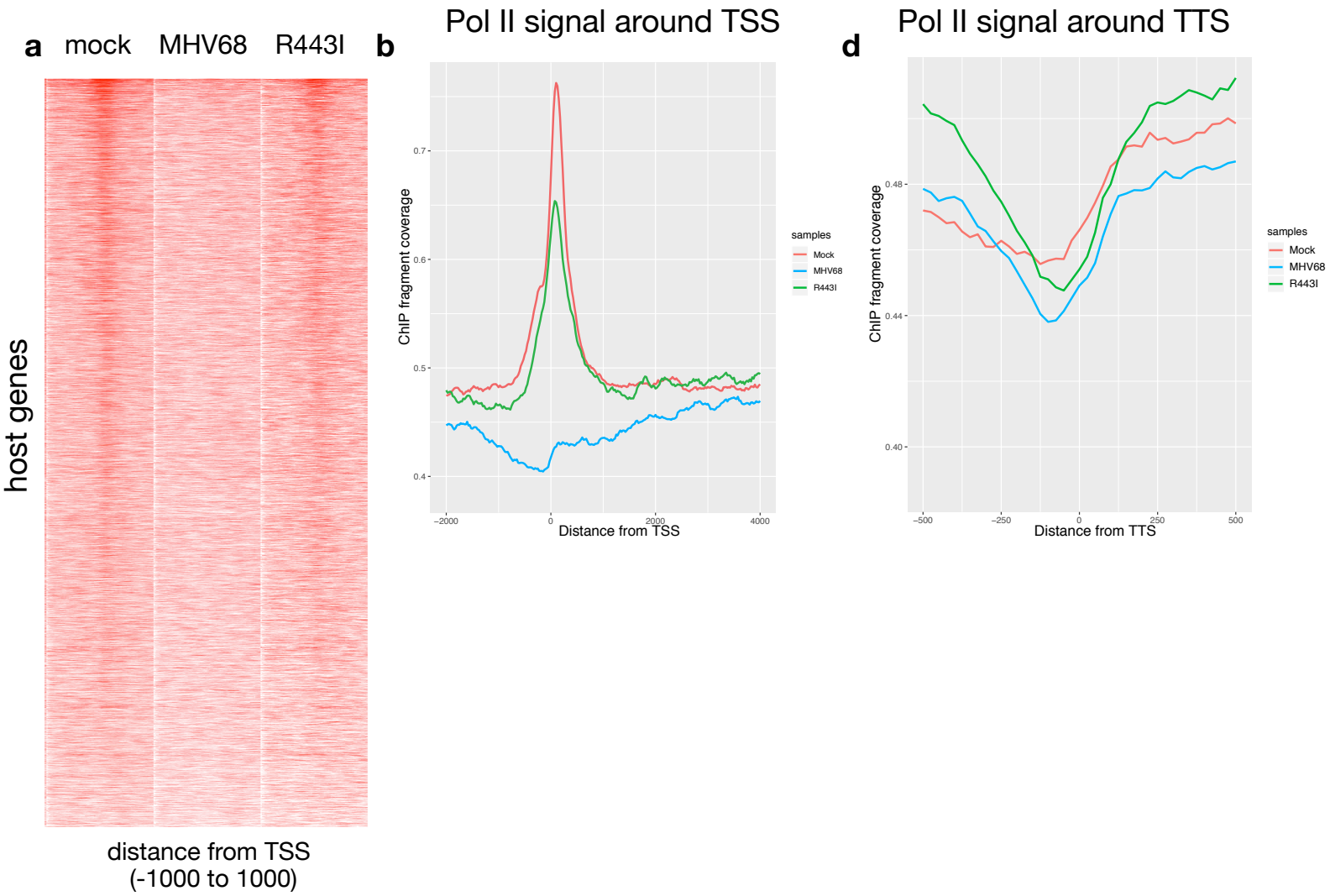

Supp Figure 2

a Unreactivated iSLKs harboring latent KSHV

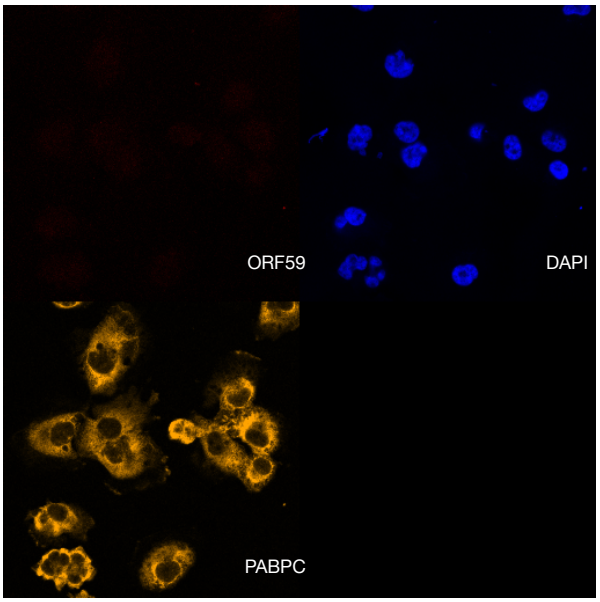
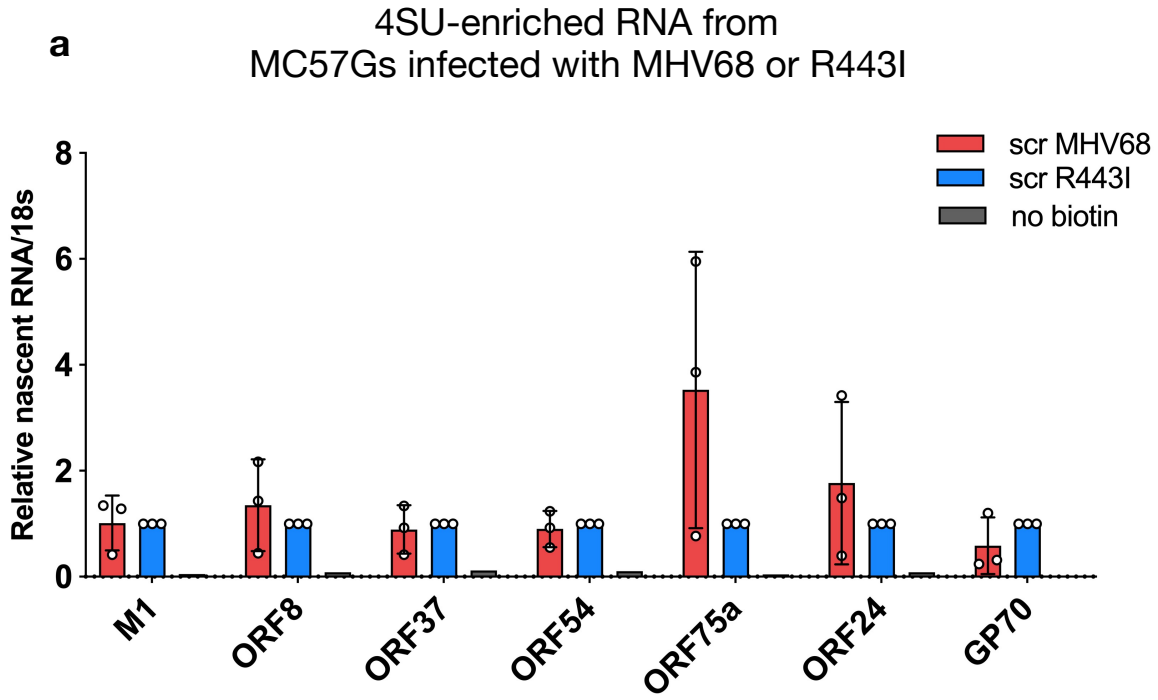
Supp Figure 3